Electronic Research Archive

ERA, 33(12): 7763–7790.
DOI: 10.3934/era.2025343
Received: 31 August 2025
Revised: 17 December 2025
Accepted: 18 December 2025
Published: 24 December 2025

https://www.aimspress.com/journal/ERA

Research article

Nonlinear cooperation between fast and slow dynamics underlying different subthreshold resonances in olive neurons model

Runxia Wang[1], Yanbing Jia[2,*] and Yuye Li[3]

[1] Department of General Education, Wuxi University, Wuxi 214105, China
[2] School of Mathematics and Statistics, Henan University of Science and Technology, Luoyang 471023, China
[3] College of Mathematics and Computer Science, Chifeng University, Chifeng 024000, China

* **Correspondence:** Email: jiayanbing@haust.edu.cn.

Abstract: Different subthreshold resonance patterns characterized by different amplitudes and frequencies are evoked from the resting potential of the medial superior olive neurons, playing important roles in sound localization. In the present paper, the conditions and nonlinear cooperation mechanisms between two ionic currents for the different patterns are obtained in a neuronal model. As the resting potential is close to the half-activation voltage of low threshold potassium current (I_{KLT}), simulation results of resonances match the experimental observations. For weak stimulation with small amplitude, slow hyperpolarization-activated cation current (I_H) is not activated, whereas fast I_{KLT} is activated to mediate a common single resonance, exhibiting small amplitude with symmetry to the resting potential and high frequency for sound localization. For strong stimulation with large amplitude, I_H is also activated to mediate a low frequency resonance and enhance the frequency of resonance mediated by I_{KLT} for precise sound localization. Then, an uncommon phenomenon of double resonances appears, which exhibits large and non-symmetrical amplitude. The different resonances are well explained with the fast frequency response of I_{KLT} and slow response of I_H. Interestingly and paradoxically, an oscillation not around its steady value appears at a high frequency of stimulation, since I_H is too slow to recover. If the time scale of two currents becomes approximate, the paradoxical oscillation disappears. Finally, for the double resonances, the phase trajectory is wide enough to cover a large part of nullclines with nonlinearity, resulting in large and asymmetrical amplitudes. For the single resonance with small and symmetrical amplitude, the trajectory is narrow to cover only a local linear part of nullcline. These results present feasible measures to modulate the high frequency response of the medial superior olive neurons for sound localization.

Keywords: subthreshold resonance; double resonances; nullcline; sound localization; fast and slow response

1. Introduction

The nonlinear dynamics of neural electrical activities play important roles in both brain functions and diseases [1–3]. For instance, membrane potential resonance serves as a key mechanism for detecting external signals with varying amplitudes or frequencies [4–9]. The subthreshold resonance means that the membrane voltage manifests a large response at a frequency [10–12]. For example, when receiving different subthreshold stimulations, the medial superior olive (MSO) neurons exhibit different subthreshold resonance patterns, characterized by different amplitudes and different frequencies, which contribute to the sound localization [7,13]. Sound localization plays important roles in seeking food, searching for offspring and parents, and avoiding predators of many species. A sound can induce a very small time-difference (~100 μs) between the two ears [12–16]. To detect the small time-difference for sound localization, the MSO manifests a resonance or firing with a high frequency around 300 Hz. Then, the high frequency response is a key clue to the sound localization [17–20], which is induced by a fast low threshold potassium current (I_{KLT}) [13]. Interestingly, the frequency mediated by the I_{KLT} is much higher than that of other neurons without I_{KLT}, such as the inferior olive neurons and other neurons [21–25]. Furthermore, a hyperpolarization-activated cation current (I_H) with slow dynamics can modulate the resonance of the MSO neurons [26], forming different resonance patterns. Then, identification of the cause for different resonance patterns, and the maintenance or enhancement of the frequency of the resonances, are favorable for accurate sound localization.

The MSO neuron is often at a resting state when not receiving stimulation, exhibiting a resting membrane potential (V_{rest}). Different resonance patterns [13,27] are induced by different external stimulations applied to the V_{rest}, exhibiting different amplitudes or different frequencies, which may be responsible for detecting different stimulations. In biological experiments, external stimulation with increasing frequency, called I_{ZAP} current, is used to evoke resonance. At an early stage, a weak stimulation with small amplitude and linearly increasing frequency is applied, and only a single resonance at a high frequency (~260 Hz) [7] is evoked, which is mediated by the fast I_{KLT}. The resonance amplitude is small, and the top and bottom envelopes of the membrane potential are symmetrical to the V_{rest} [27], similar to the common resonance widely observed in various neurons [21,28,29]. Then, as the I_{ZAP} becomes strong, although still a single resonance is evoked, the amplitude becomes large and asymmetrical to the V_{rest}, behaving as a depolarization resonance [13]. Recently, as the frequency of the large I_{ZAP} increases exponentially, double resonances with large and asymmetrical amplitudes appear. One resonance exhibits a depolarization amplitude and high frequency ~300 Hz, mediated by the fast I_{KLT} [26,30]. The other resonance manifests hyperpolarization amplitude and low frequency ~50 Hz, mediated by the slow I_H. Furthermore, compared with the single resonance for a weak stimulation, the depolarization resonance exhibits a higher frequency, implying more accurate sound localizations. For the double resonances, the top and bottom envelopes of the voltage response are asymmetrical to the V_{rest} [26,30]. In addition, as I_H is blocked, a single depolarization resonance with large and asymmetrical amplitude appears. Such an asymmetrical resonance has attracted much less attention, in addition to an interesting study [27], wherein an asymmetrical resonance is regarded as an uncommon phenomenon the resonance. Different from the MSO, the asymmetrical resonance is

mediated by a slow outward potassium current (I_M). Furthermore, the asymmetrical amplitudes are effectively analyzed with a novel geometric analysis method and compared with the symmetrical amplitude: the asymmetrical are related to the nonlinear parts of the nullclines related to I_M, and the symmetrical amplitude is induced by the linear nullcline. Paradoxically, a phenomenon that the resonance behavior does not oscillate around the steady state value of one variable is observed. However, the dynamical mechanism for the paradoxical remains unclear. Then, such a novel geometric method for only one ionic current (I_M) may be extended to recognize the asymmetrical resonance of the MSO, which may be associated with nullclines for two ionic currents (I_M and I_{KLT}).

Despite these progresses, several questions remain unclear. For instance, for a weak stimulation, why does high frequency resonance mediated by I_{KLT} appear, and why does not low frequency resonance mediated by I_H appear? The cooperation between V_{rest} and activation of the I_{KLT} and the I_H may be the cause. In addition, although the cooperation between the dynamics of I_{KLT} and I_H to modulate the double resonances for strong stimulation has been acquired [30], the cooperation between the I_{KLT} and I_H to modulate the single resonances for weak stimulation remains unclear. Furthermore, the cause of the uncommon phenomenon of the asymmetrical amplitudes is still an open problem, due to a lack of an analysis method. Then, the geometric analysis in the study [27] may be extended as an effective method to analyze the nonlinear dynamics underlying different resonance patterns modulated by the two ionic currents. Furthermore, is there a paradoxical phenomenon that the resonance behavior does not oscillate around the steady state value of a variable? If there is, what is the condition or dynamical mechanism for the paradoxical phenomenon? The answers to these questions are very important for the dynamics of MSO neurons, sound localization, and nonlinear phenomena across in engineering and natural sciences.

The questions mentioned above are investigated in a neuronal model in the present paper. First, conditions for the different resonance patterns are obtained. The activation of the I_{KLT} and I_H and their relationships to the V_{rest} are presented, and the time scales of the I_{KLT} and I_H are provided, closely matching the experimental conditions. Second, different resonance patterns are reproduced for stimulation with different amplitudes. As stimulation amplitude increases, single resonance with a symmetrical/small amplitude and high frequency changes to double resonances with asymmetrical and large amplitude, accompanied by enhancement of the high frequency of the resonance that facilitates sound localization. Third, the different resonance patterns are explained with cooperations between different activations and different frequency responses of fast I_{KLT} and slow I_H. The single resonance is dominated by the response of I_{KLT} at high frequency and the inactivation of I_H. However, for double resonances, I_H current is activated at slow frequency, which can mediate the resonance for low frequency and induce the high frequency of the resonance mediated by I_{KLT} enhanced. Interestingly and paradoxically, an oscillation that is not around its steady value appears at a high frequency of stimulation, since I_H is too slow to recover within a relatively short stimulation period. Such a behavior shows complex dynamics of frequency response induced by the frequency mismatch between external stimulation and internal factors. If the time scale of I_{KLT} and I_H becomes approximate, the paradoxical oscillation disappears. Finally, the novel geometric analysis method is extended to explain the symmetrical characteristic of the amplitude. The asymmetrical amplitude is large enough to cover a large part of nullclines which exhibit nonlinearity, and the symmetrical amplitude is small enough to only cover a local part of nullclines which manifest linearity. These results provide the nonlinear and ionic current mechanisms of the different resonance patterns, which not only help to regulate the resonance of MSO neurons, but also to facilitate the sound localization.

2. Models and methods

2.1. MSO neuron model

In addition to the positive currents such as the sodium current (I_{Na}) and hyperpolarization-activated cation current (I_H), the MSO neuron model [13] also contains negative currents, such as the high-threshold potassium current (I_{KHT}), low-threshold potassium current (I_{KLT}), and leak current (I_L). The model equations are as follows:

$$C_m \frac{dV}{dt} = \sum I = -g_{Na} m^3 h(V - E_{Na}) - g_{KHT}(0.85n^2 + 0.15p)(V - E_K) - g_{KLT} w^4 z(V - E_K) - g_H r(V - E_h) - g_L(V - E_L) + I_{\mathrm{DC}}, \tag{1}$$

$$\frac{dx}{dt} = \frac{x_\infty - x}{\tau_x(V)}, \tag{2}$$

where the parameter C_m is the membrane capacitance, and the variable V represents the membrane voltage. The symbol x denotes 7 gating variables m, h, n, p, w, z, and r. The variables m and h represent the activation and inactivation of I_{Na}, respectively, n and p correspond to the activation and inactivation of I_{KHT}, respectively, w and z are the activation and inactivation of the I_{KLT}, respectively, and r is the inactivation of I_H. The parameters g_{Na} = 1275 nS, g_{KHT} = 150 nS, g_{KLT} =190 nS, g_H = 70 nS, and g_L =15 nS are the maximal conductances, while E_{Na} = 55 mV, E_K = –106 mV, E_H = –37 mV, and E_L = –77.5 mV are the Nernst potentials. These parameters were selected based on [13] and the electrophysiological experiments described in [19]. The parameter I_{DC} = 0.176 nA is a constant current. The functions $x_\infty(V)$ and $\tau_x(V)$ ($x = m, h, n, p, w, z$, and r) are the steady-state function and time constant, respectively, which are described as follows:

$$w_\infty = \frac{1}{1+e^{-(V+57.3)/11.7}},\ z_\infty = \frac{0.78}{1+e^{(V+57)/5.44}} + 0.22,\ \ r_\infty = \frac{1}{1+e^{(V+76)/7.3}},$$

$$m_\infty = \frac{1}{1+e^{-(V+38)/7}}, h_\infty = \frac{1}{1+e^{(V+65)/6}}, n_\infty = \frac{1}{[1+e^{-(V+15)/5}]^{1/2}}, p_\infty = \frac{1}{1+e^{-(V+23)/6}},$$

$$\tau_m = \frac{0.24 \cdot 10}{5e^{(V+60)/18} + 36e^{-(V+60)/25}} + 0.04 \cdot 0.24,\ \tau_n = \frac{0.24 \cdot 100}{11e^{(V+60)/24} + 21e^{-(V+60)/23}} + 0.7 \cdot 0.24,$$

$$\tau_p = \frac{0.24 \cdot 100}{4e^{(V+60)/32} + 5e^{-(V+60)/22}} + 5 \cdot 0.24,\ \tau_p = \frac{0.24 \cdot 100}{4e^{(V+60)/32} + 5e^{-(V+60)/22}} + 5 \cdot 0.24,$$

$$\tau_z = 0.24\left[\frac{1000}{e^{-(V+60)/20} + e^{-(V-60)/8}} + 50\right].$$

In the present paper, we focus on subthreshold resonance mediated by the I_H and I_{KLT} currents. I_H is a hyperpolarization-activated cation current widely distributed in the nervous system and serves important functions. For example, research indicates that I_H contributes to enhancing the coding accuracy of sound localization. I_H current exhibits slow kinetic properties and can induce subthreshold resonance at approximately 6 Hz in hippocampal pyramidal neurons [23]. I_{KLT} is a low-threshold potassium current commonly found in the auditory system, and its fast kinetic characteristics are crucial for nuclei involved in sound localization, such as the superior olivary complex. This paper adopts a model based on electrophysiological experiments conducted on brainstem neurons [19]. In

the model [19], the expressions for the time constants of I_H and I_{KLT} are as follows:

$$\begin{aligned}\tau_r &= [\frac{0.24\cdot 100}{7e^{(V+60)/11}+36e^{-(V+60)/25}}+0.6\cdot 0.24],\\ \tau_w &= 0.46[\frac{100}{6e^{(V+75)/12.15}+24e^{-(V+75)/25}+0.55}].\end{aligned} \tag{3}$$

In this study, the time constant reflects the inactivation and activation rate of ionic channel. In this study, the range of time constants are studied. Then, coefficients α_H and β_{KLT} are added to the equations of time constant to represent the scale of time constant, as described as follows:

$$\begin{aligned}\tau_r &= \alpha_H[\frac{0.24\cdot 100}{7e^{(V+60)/11}+36e^{-(V+60)/25}}+0.6\cdot 0.24],\\ \tau_w &= \beta_{KLT}[\frac{100}{6e^{(V+75)/12.15}+24e^{-(V+75)/25}+0.55}].\end{aligned} \tag{4}$$

The coefficient α_H was varied over the range of 0.01 to 0.3, and β_{KLT} over the range of 0.11 to 0.35.

2.2. I_{ZAP} current to induce resonance

In many studies [23,27,29], the single resonance is evoked by an I_{ZAP} with frequency changed linearly, which is described as follows:

$$\begin{aligned}I_{ZAP}(t) &= A_{in}\sin[2\pi f(t)t)],\\ f(t) &= f_s+(f_e-f_s)\frac{t}{T},\end{aligned} \tag{5}$$

where f_s represents the starting frequency, f_e is the ending frequency, and T is the duration of the stimulus. In fact, the resonance frequency should be located within the range between f_s and f_e, and T should be long enough to ensure that there is a period to capture the resonance.

However, only when T is very long, double resonances respectively at a low frequency and a high frequency can be evoked or captured. When plotted in a figure, the time solution of the period of I_{ZAP} is low, since the very long T. To enhance the time solution of the figure, an I_{ZAP} with frequency changed exponentially instead of linearly can induce or capture the double resonances, even when T is relatively short, which was used in the experimental study [26]. Inspired by the experimental study [26], such an I_{ZAP} is used in the present paper and is described as follows:

$$I_{ZAP}(t) = A_{in}\sin[\phi(t)], \tag{6}$$

$$\phi(t) = \frac{(2\pi)f_sT}{\ln(f_e/f_s)}(\frac{f_e}{f_s})^{t/T}, \tag{7}$$

where A_{in} and $\phi(t)$ are the amplitude of stimulation and phase function, respectively. The time factor t

is contained in the item $f_s\left(\frac{f_e}{f_s}\right)^{t/T}$ in Eq (7). The derivative of $\phi(t)$ corresponds to the spontaneous frequency of $I_{ZAP}(t)$, which is labeled as $f_{in}(t)$ and is described as follows:

$$f_{in}(t) = \frac{1}{2\pi}\frac{d\phi(t)}{dt} = f_s(\frac{f_e}{f_s})^{t/T}. \tag{8}$$

In the present paper, the values of f_s, f_e, and T are 10 Hz, 850 Hz, and 20 s, respectively. A_{in} is chosen as control parameter. A small value or a large value of A_{in} corresponds to weak stimulation or strong stimulation, respectively.

A representative example of I_{ZAP} with A_{in} = 0.05 nA is shown by the black curve in the middle part of Figure 1. Especially, the blue curve in the bottom represents the exponential change of frequency, $f_{in}(t)$, differing from the common I_{ZAP} with linearly changing frequency. In fact, for the latter part of I_{ZAP}, the time solution of period is low. Then, the top 3 inset panels (black, magenta, and green curves) represent the enlargement of I_{ZAP} current corresponding to the timing labeled with the three arrows, respectively. Two cycles of I_{ZAP} around 0.4 s, 10 s, and 19.5 s are presented, respectively, showing a high time solution of period.

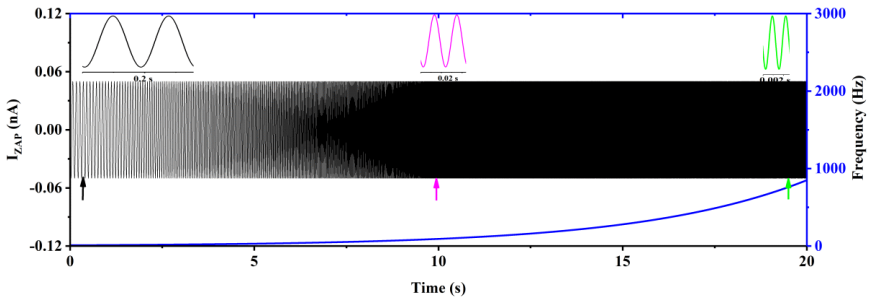

Figure 1. The I_{ZAP} current (black) with exponential frequency for small amplitude A_{in} = 0.05 nA and changes of frequency (blue curve). Within 20 s, 10 Hz changes to 850 Hz. The top 3 inset panels (black, magenta, and green curves) represent the two cycles of the I_{ZAP} current corresponding to the timing labeled with the three arrows, respectively.

During the continuous changes of frequency of I_{ZAP}, the resonance within the frequency range of I_{ZAP} can be captured easily (Figures 3, 5, 12, 14, and 17 of the present paper). In fact, there is no correspondence of I_{ZAP} in real neurons, whether linear changing frequency or exponential changing frequency, since I_{ZAP} is a manner to evoke the resonances which exist in the frequency range of I_{ZAP}. Then, after capturing the resonance induced by I_{ZAP}, more detailed dynamics of the resonance are further investigated at fixed frequencies (Figures 8–11, 15, and 16). I_{ZAP} is a practical manner to capture resonance in the biological experiments, whereas the dynamics of resonance at fixed frequencies corresponds to real neurons.

2.3. Measure to characterize the symmetry of the resonance

The MSO neuron stimulated by I_{ZAP} is described as follows:

$$C_m \frac{dV}{dt} = \sum I = -g_{Na} m^3 h(V - E_{Na}) - g_{KHT}(0.85n^2 + 0.15p)(V - E_K) - g_{KLT} w^4 z(V - E_K) - g_H r(V - E_h) - g_L(V - E_L) + I_{\mathrm{DC}} + I_{ZAP}, \quad (9)$$

$$\frac{dx}{dt} = \frac{x_\infty - x}{\tau_x(V)}. \quad (10)$$

If I_{ZAP} is ignored, the membrane potential $V(t)$ is at resting state and is labeled as V_{rest}. After introducing I_{ZAP} current with amplitude A_{in}, $V(t)$ exhibits oscillations. The envelopes of $V(t)$ are used to characterize the symmetry of the resonance induced by I_{ZAP}, according to [27]. For $V(t)$ evoked from V_{rest}, the local maximal values on the upper envelope are labeled as $V_{max}(t)$ and the minimal values on the lower envelope as $V_{min}(t)$. $V_{max}(t) - V_{\mathrm{rest}}$ is labeled as $V^+(t)$, and the absolute values of $| V_{min}(t) - V_{\mathrm{rest}} |$ is labeled as $V^-(t)$. Then, for the amplitude A_{in}, normalize $V^+(t)$ and $V^-(t)$ by dividing A_{in} to acquire the impedance profiles

$$Z(f)^{+/-} = \frac{V^{+/-}}{A_{in}}, \quad (11)$$

where $Z(f)^+$ and $Z(f)^-$ respectively correspond to the depolarization and hyperpolarization impedance profiles. The resonances can be classified into different patterns according to the relationships between $Z(f)^-$ and $Z(f)^+$:

1) If $Z(f)^-$ nearly coincides with $Z(f)^+$, the resonance is called resonance with symmetrical amplitude. If $Z(f)^-$ does not coincide with $Z(f)^+$, the resonance is called asymmetrical resonance.

2) If the peaks of $Z(f)^-$ and $Z(f)^+$ occur at nearly a same frequency or only one of $Z(f)^-$ and $Z(f)^+$ has a peak, a single resonance appears. If the peak of $Z(f)^-$ appears at a frequency significantly different from that of $Z(f)^+$, the resonances are called double resonances.

2.4. Geometrical analysis to show the asymmetrical amplitude of resonance

In the study [27], the phase trajectory of the response behavior and the nullclines in the phase plane were used to study the asymmetrical amplitude of the resonance mediated by a single current. In the present paper, such a method is extended to characterize the symmetrical or asymmetrical amplitudes of the different resonance patterns mediated by two different resonance currents.

For the resonance induced by an external signal $A\sin(2\pi ft)$ with a fixed frequency f, the first equation is changed to $C_m \frac{dV}{dt} = \sum I + A\sin(2\pi ft)$. Then, three V-nullclines $\frac{dV}{dt} = 0$ are acquired, which are $C_m \frac{dV}{dt} = \sum I + A = 0$, $C_m \frac{dV}{dt} = \sum I = 0$, and $C_m \frac{dV}{dt} = \sum I - A = 0$, corresponding to peak, 0, and trough of $A\sin(2\pi ft)$, respectively. In addition, r-nullcline $r = r_\infty(V)$ for the I_H to mediate the hyperpolarization resonance and w-nullcline $w = w_\infty(V)$ for the I_{KLT} to mediate the depolarization resonance are acquired. Considering that $I_{KLT} = -g_{KLT} w^4 z(V - E_K)$ and w^4 determines the instantaneous conductance of the I_{KLT}, w^4 instead of w and w_∞^4 instead of w_∞ are used in the phase

plane. Then, the phase trajectory of the response behavior at different frequencies f is projected to the phase planes (V, r) and (V, w^4). The locations of the phase trajectory, equilibrium point, and nullclines, the shape of nullclines (nearly linear or nonlinear), and the symmetry of the nullclines to the V_{rest}, are used to explain the symmetrical or asymmetrical amplitude of the resonance and the changes of symmetrical characteristics with respect to stimulations.

2.5. Method

The theoretical model is solved by the fourth-order Runge–Kutta algorithm, and a time step 0.001 ms is used.

3. Results

3.1. Dynamics of the I_{KLT} and I_H currents

3.1.1. Nonlinear activation function of the I_{KLT} and I_H currents

The blue curve and magenta curve in Figure 2(a) represent the steady-state function of activation variable w of the I_{KLT} ($w_\infty(V) = \frac{1}{1+e^{-(V+57.3)/11.7}}$,) and of r of the I_H ($r_\infty(V) = \frac{1}{1+e^{(V+76)/7.3}}$), respectively. The red horizontal dashed line corresponds to half-activation (0.5) of activation variables. The magenta solid circle and blue solid circle represent the half-activation voltages for $r_\infty(V)$ and $w_\infty(V)$, labeled as $V_{1/2,r}$ and $V_{1/2,w}$, and the values are −76 mV and −57.3 mV, respectively.

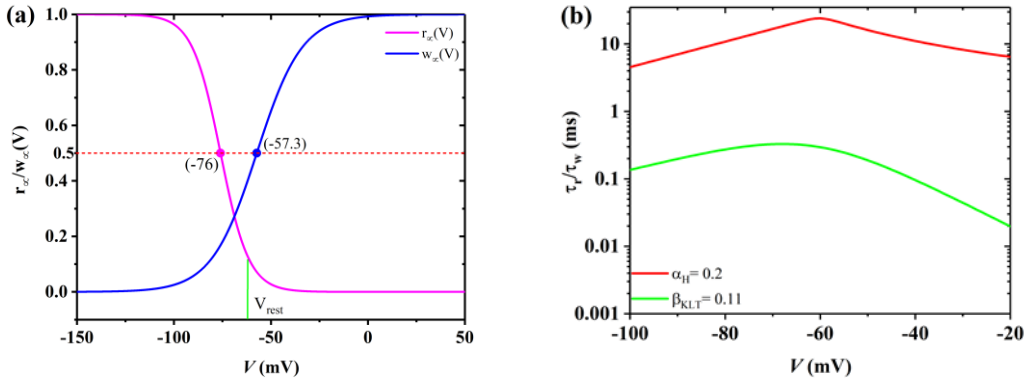

Figure 2. Dynamics of the I_{KLT} and I_H. (a) $r_\infty(V)$ (magenta) for the I_H and $w_\infty(V)$ (blue) for the I_{KLT}. The green vertical line denotes V_{rest}; (b) The changes of time constant τ_r for $\alpha_H = 0.2$ (red) of the I_H and τ_w for $\beta_{KLT} = 0.11$ (green) of the I_{KLT} with respect to V.

3.1.2. The level of resting state

In the present paper, the resting membrane potential $V_{\text{rest}} = -62$ mV is shown by the green vertical line in Figure 2(a). Obviously, $V_{\text{rest}} = -62$ mV is close to $V_{1/2,w} = -57.3$ mV (blue circle) for the I_{KLT} and far from $V_{1/2,r}$ (magenta circle) for the I_H. Such a value of V_{rest} ensures the activation of I_{KLT} and

inactivation of I_H for weak stimulation, which is the cause for the resonance mediated by I_{KLT} for weak stimulation. The detailed results please refer to Subsection 3.2. If V_{rest} is close to $V_{1/2,r}$ = –76 mV, I_H is activated for weak stimulation, whereas I_{KLT} is not for small amplitude. Then, single resonance mediated by the I_H should appear (simulation result is not shown here), which is consistent with the experimental observation of resonance in other neurons [23]. Then, V_{rest} = –62 mV is chosen in the present paper. The results are similar when V_{rest} is around –62 mV.

3.2. Different resonance patterns

3.2.1. Single resonance with symmetry for different time scales of the I_H and I_{KLT}

Single resonance with symmetrical amplitude for different time constants (α_H and β_{KLT}) induced by a weak stimulation A_{in}= 0.05 nA is shown in Figure 3, with the values of α_H and β_{KLT} shown in each panel. The resonance exhibits a single frequency, amplitude with symmetry, a small amplitude, and a high frequency (~240–300 Hz). The results of Figure 3 show that the single resonance with symmetrical amplitude appears in a wide range of time scales of the two resonance currents.

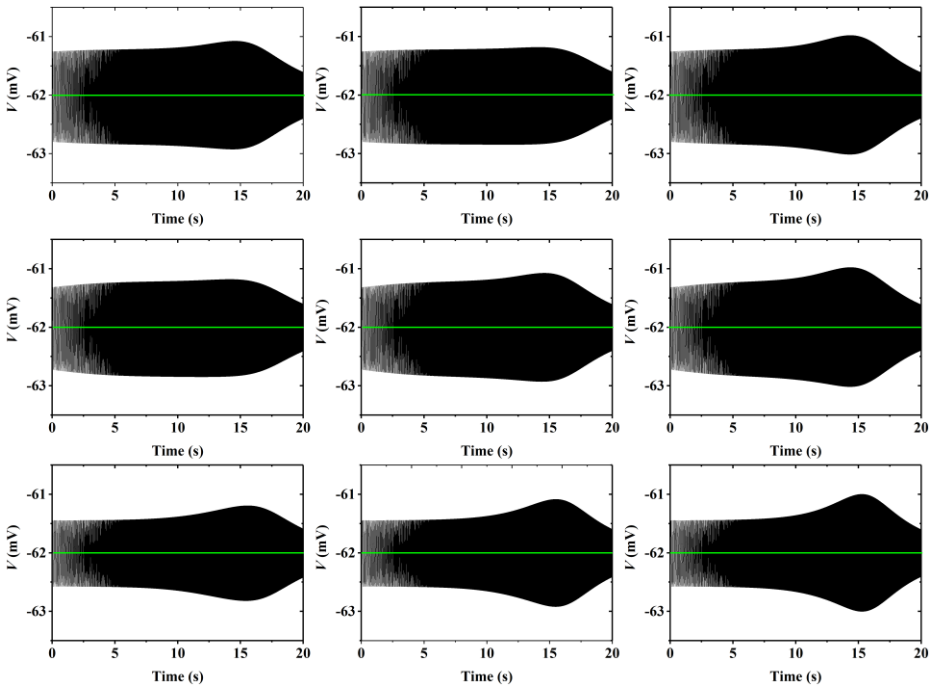

Figure 3. The single resonance with symmetrical and small amplitude at different values at α_H and β_{KLT} to modulate time constants. Top row: α_H = 0.4; Middle row: α_H = 0.2; Bottom row: α_H = 0.01. Left column: β_{KLT} = 0.11; Middle column: β_{KLT} = 0.17; Right column: β_{KLT} = 0.23.

To clearly show the symmetrical amplitude of the resonance, taking the first in the middle row of Figure 3 as an example, the impedance profiles of the voltage response are shown in Figure 4, denoted by black solid ($Z(f)^+$) and dashed ($Z(f)^-$) curves, respectively. For the single resonance with symmetrical amplitude, $Z(f)^+$ and dashed $Z(f)^-$ almost coincide, thus $|Z(f)^- - Z(f)^+|$ approximates 0, as

shown by the horizontal magenta line in Figure 4. For I_{ZAP} current with a small amplitude (A_{in} = 0.05 nA), the resonance exhibits a single frequency, an amplitude symmetrical to V_{rest} (green line), and a small amplitude (about 2 mV). The frequency of resonance is ~243 Hz.

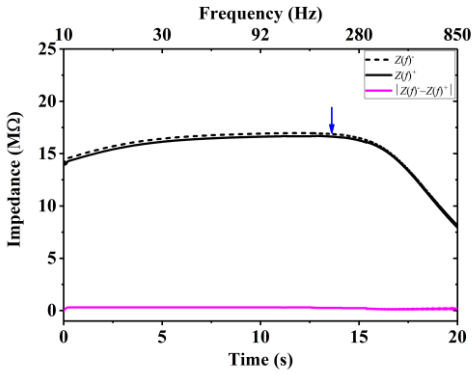

Figure 4. Impedance profiles of single resonance with small and symmetrical amplitude for weak stimulation amplitude with A_{in} = 0.05 nA, α_H = 0.2, and β_{KLT} = 0.11; The bottom X-axis represents time, while the top X-axis displays the corresponding frequency. The black solid and dashed curves represent $Z(f)^+$ and $Z(f)^-$, respectively, and the magenta solid curve represents $|Z(f)^- - Z(f)^+|$.

3.2.2. Double resonances with asymmetrical amplitude induced by strong stimulations

As the amplitude of the subthreshold I_{ZAP} increases to large values, the single resonance with symmetrical and small amplitudes changes to the double resonances with large and asymmetrical amplitudes.

For middle amplitude (A_{in} = 0.2 nA), the voltage response exhibits double resonances with a middle amplitude (~7 mV), as depicted in Figure 5(a1). One resonance exhibits a low frequency and hyperpolarization amplitude (blue arrow), and the other a high frequency and depolarization amplitude (red arrow). The frequency of the depolarization resonance is ~273 Hz for the middle amplitude. For strong stimulation A_{in} = 0.7 nA, double resonances with large amplitude (~20 mV) appear, as shown in Figure 5(a2). The double resonances closely match the experimental result [26]. The frequency of the depolarization resonance is ~342 Hz for the strong stimulation, showing that the stimulation amplitude enhances the resonance frequency. Then, the result implies that the sound source with a larger amplitude is easier to be localized. In this study, we primarily focus on the effects of the amplitude of the stimulus current I_{ZAP} and the timescales of I_H and I_{KLT} on the resonance pattern. The conductances of I_H and I_{KLT} were set to 70 nS and 190 nS, respectively. In fact, increasing or decreasing g_{KLT} or g_H by approximately 20% within a certain range may alter the frequency and amplitude of resonance but does not induce a transition in the resonance pattern (not shown here).

The impedance profiles $Z(f)^+$ and $Z(f)^-$ are shown in Figures 5(b1) and (b2). The magenta solid curve represents $|Z(f)^- - Z(f)^+|$ to show the asymmetrical degree, showing non-zero values in a wide frequency range. Then, the double resonances for the middle and strong stimulations exhibit asymmetrical amplitude. The magenta curve in Figure 5(b2) is larger than that in Figure 5(b1) in a wide range, showing that the asymmetrical degree of the double resonances induced by a strong

stimulation (Figure 5[a2] and [b2]) is larger than that induced by a stimulation with middle amplitude (Figure 5[a1] and [b1]).

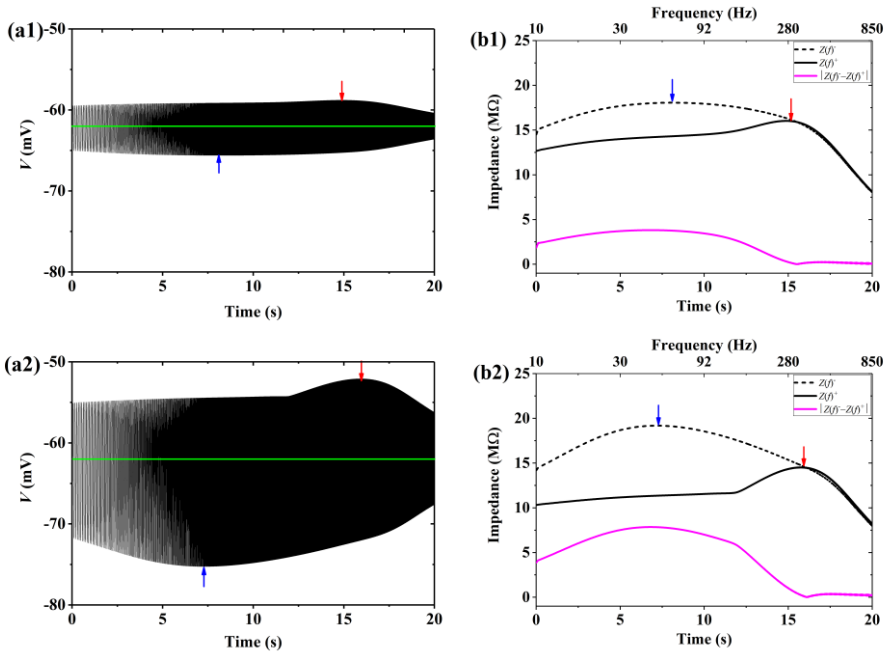

Figure 5. Frequency responses of the resting membrane potential $V_{\text{rest}} = -62$ mV, $\alpha_H = 0.2$, $\beta_{KLT} = 0.11$ to I_{ZAP} current with different amplitudes. (a1) Double resonances with middle and asymmetrical amplitude for middle stimulation amplitude A_{in} = 0.2 nA; (b1) Impedance profiles of panel (a1); (a2) Double resonances with large and asymmetrical amplitude for strong stimulation amplitude $A_{in} = 0.7$ nA; (b2) Impedance profiles of panel (a2). In the right column, the black solid and dashed curves represent $Z(f)^+$ and $Z(f)^-$, respectively, and the magenta solid curve represents $|Z(f)^- - Z(f)^+|$. The bottom x-axis represents time, while the top x-axis displays the corresponding frequency.

3.2.3. The dependence of depolarization and hyperpolarization resonance on stimulation amplitude, β_{KLT} of I_{KLT}, and α_H of I_H

The changes of depolarization resonance frequency with increasing stimulation amplitude A_{in} and the time constant β_{KLT} of I_{KLT} are shown in Figure 6. As illustrated in Figure 6(a), the resonance frequency increases with increasing stimulation amplitude A_{in} and decreasing the time constant β_{KLT} of I_{KLT}. Then, increasing amplitude A_{in} and decreasing time constant β_{KLT} present potential measures to enhance the depolarization resonance frequency. Figure 6(b) shows the hyperpolarization resonance frequency. At the down-right part of Figure 6(b), the frequency is relatively high, and there is small difference to the depolarization resonance frequency (Figure 6(a)). At the up-left part of Figure 6(b), the frequency is low, which is much lower than that of the depolarization resonance (Figure 6(a)). Then, the double resonances appear in the up-left part, and the single resonance in the down-right part,

as shown in Figure 6(c). The difference between the depolarization resonance frequency and hyperpolarization resonance frequency is larger than 30 Hz for the double resonances. In addition, the weak, middle, and strong stimulations can be distinguished to a certain extent, according to Figure 6. In Figure 6(a), the most part of green area, the most part of yellow area and up-right part of green area, and the red part correspond to weak, middle, and strong stimulations, respectively.

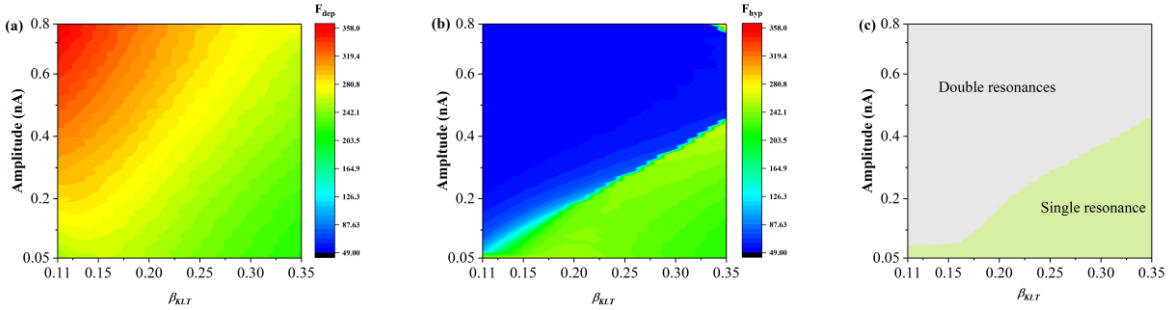

Figure 6. The change of resonance frequency with the variations in stimulation amplitude A_{in} and the time constant β_{KLT} of I_{KLT}. (a) Depolarization frequency in the plane (β_{KLT}, A_{in}); (b) Hyperpolarization resonance frequency in the plane (β_{KLT}, A_{in}); (c) The distribution of single and double resonances in the plane (β_{KLT}, A_{in}). The gray represents double resonances and light green represents single resonance.

The change of depolarization resonance frequency with increasing stimulation amplitude A_{in} and the time constant α_H of I_H are shown in Figure 7. As depicted in Figure 7(a), the resonance frequency increases with increasing A_{in} and changes little with increasing α_H. Then, increasing amplitude A_{in} presents a potential measure to enhance the depolarization resonance frequency. Figure 7(b) shows the changes of hyperpolarization resonance frequency. At the bottom or left part, the frequency is relatively high. At the remaining part, the frequency is low, which is much lower than that of the depolarization resonance (Figure 7(a)). Except the down-left corner, there is obvious difference between the frequencies of depolarization resonance and hyperpolarization resonance (Figure 7(a)). Then, the single resonance appears in the down-left corner, and double resonances appear in the other part, as shown in Figure 7(c). The difference between the depolarization resonance frequency and hyperpolarization resonance frequency is larger than 30 Hz for the double resonances. In our previous study [30], the ionic mechanism that the I_H enhances the frequency of resonance mediated by I_{KLT} for large-amplitude stimulation is obtained. In the present paper, the mechanism for middle and weak stimulation are similar (not shown here to avoid repetition).

In summary, the amplitude of the I_{ZAP} current and the time scales of the I_H and I_{KLT} currents are key factors influencing the transition of resonance patterns. When the I_H current is slow (i.e., with a large α_H) and the I_{KLT} current is fast (i.e., with a small β_{KLT}), an increase in stimulus amplitude causes the resonance pattern to shift from single to double resonances, as illustrated in Figures 6(c) and 7(c). At strong stimulus amplitudes, if the time scale of the I_H current becomes faster (i.e., α_H decreases)

while that of the I_{KLT} current becomes slower (i.e., β_{KLT} increases), the resonance pattern changes from double back to single resonance.

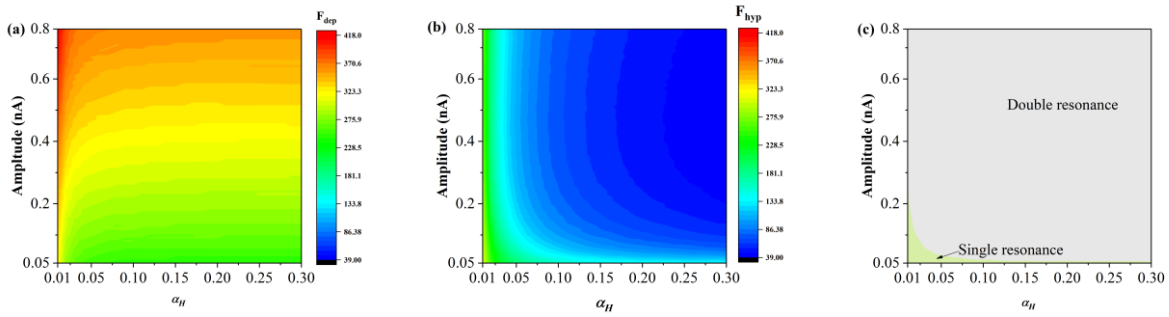

Figure 7. The change of resonances frequency with the variations in stimulation amplitude A_{in} and the time constant α_H of I_H. (a) Depolarization resonances frequency in the plane (α_H, A_{in}); (b) Hyperpolarization resonances frequency in the plane (α_H, A_{in}); (c) The distribution of single and double resonances in the plane (α_H, A_{in}). The gray represents double resonances and light green represents single resonance.

3.3. The cooperations between I_{KLT} and I_H for different resonance patterns

3.3.1. Single resonance: Low activation of I_H and fast frequency response of I_{KLT}

In fact, during the process to change the frequency of the I_{ZAP} to evoke the resonance, the responses of the I_{KLT} and I_H cannot keep up with the I_{ZAP} at different speeds, resulting in a phase difference between $V(t)$ and variables of the I_{KLT} and I_H. The I_{KLT} and I_H show different phase differences due to the different time scales. To clearly show the frequency responses of $w(t)$ and $w_\infty(t)$ of the I_{KLT}, $r(t)$ and $r_\infty(t)$ of the I_H, and $V(t)$ at different frequencies, the responses to a stimulation $A\sin(2\pi ft)$ are studied, with A = 0.05 nA and f fixed at four different values, 0.1, 50, 243, and 1500, as shown in Figure 8.

As depicted in the top row of Figure 8, $V(t)$ (black) exhibits small oscillations, and the resonance (largest amplitude) appears at f = 243 Hz, as shown in the third panel. The I_{KLT} is activated, resulting in that $w(t)$ is around 0.4, as depicted by the purple curve in the middle row. However, the I_H is nearly inactivated, resulting in $r(t)$ manifesting a small value (0.12 and 0.14), as depicted by the black dashed line in the bottom row. The activations are determined by that V_{rest} = –62 mV is close to $V_{1/2,w}$, and far from $V_{1/2,r}$, as shown in Figure 2(a).

Compared with the first and second columns, $w(t)$ exhibits a faster frequency response than $r(t)$. For a very slow frequency (0.1 Hz), $w(t)$ (purple dashed curve) can keep up with $w_\infty(t)$ (cyan solid curve), and meanwhile $r(t)$ (black dashed curve) can keep up with $r_\infty(t)$ (green curve), as shown in the first column. For a low frequency (50 Hz), $w(t)$ nearly keeps up with $w_\infty(t)$, whereas $r(t)$ cannot keep up with $r_\infty(t)$, as shown in the second column. $r(t)$ delays than $r_\infty(t)$ and $V(t)$, since $r_\infty(t)$ and $V(t)$ have the same phase. At the resonance frequency (243 Hz), $w(t)$ decreases to a small extent, whereas $r(t)$ decreases to a large extent. Then, the resonance is mainly determined by $w(t)$. For a large frequency (1500 Hz), $w(t)$ decreases to a large extent, whereas r shrinks to $r_\infty(V_{\text{rest}})$. Obviously, the

I_{KLT} exhibits a faster frequency response than the I_H current.

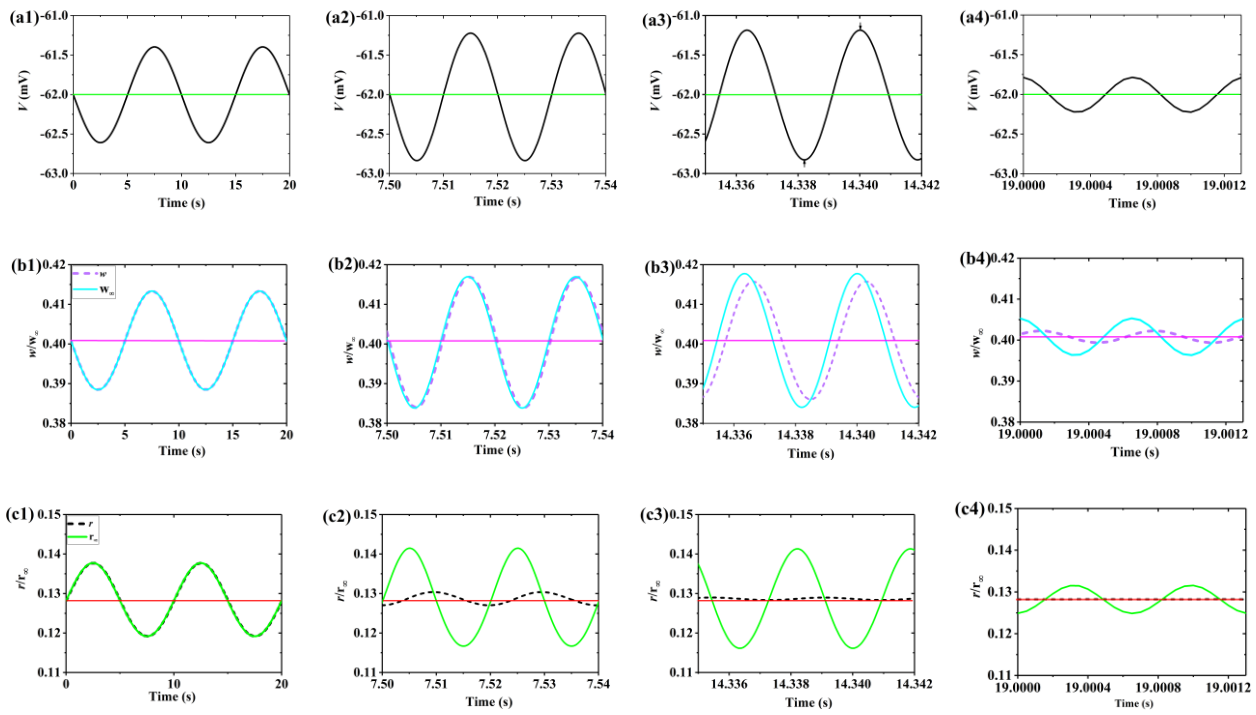

Figure 8. $V(t)$(top), $w(t)$ and $w_\infty(t)$ (middle), and $r(t)$ and $r_\infty(t)$ (bottom) at different frequencies for A = 0.05 nA. (a1), (b1), and (c1): 0.1 Hz; (a2), (b2), and (c2): 50 Hz; (a3), (b3), and (c3): 243 Hz; (a4), (b4), and (c4): 1500 Hz. The solid black curve and green line in the top row represent $V(t)$ and V_{rest}, respectively. The dashed purple, cyan, and magenta in the middle row represent $w(t)$, $w_\infty(t)$, and $w_\infty(V_{\text{rest}})$, respectively. The dashed black, solid green, and red in the bottom row represent $r(t)$, $r_\infty(t)$, and $r_\infty(V_{\text{rest}})$, respectively.

3.3.2. Double resonances: fast response of I_{KLT} and slow response of I_H

As the amplitude of the subthreshold I_{ZAP} stimuli increases to large values, the single resonance with symmetrical and small amplitude changes to the double resonances with large and asymmetrical amplitudes. As depicted in Figure 9, $V(t)$ (black) exhibits large oscillations in the top row. Double resonances appear respectively at f = 50 and 342 Hz, as shown in the second and third panels.

The $w(t)$ (purple dashed curve), $w_\infty(t)$ (cyan solid curve), and $w(V_{\text{rest}})$ (magenta) of the I_{KLT} at four f values, 0.1 Hz, 50 Hz, 342 Hz, and 1500 Hz, are shown in the upper row of Figure 9. And $r(t)$ (black dashed), $r_\infty(t)$ (green solid), and $r(V_{\text{rest}})$ (red solid) of the I_H are depicted in the lower row. Compared with the two rows, several characteristics can be found:

1) Both the I_{KLT} and the I_H current are activated, then, both $w(t)$ and $r(t)$ can reach relatively large values;

2) $w(t)$ exhibits a faster frequency resonance than $r(t)$. At the hyperpolarization resonance frequency 50 Hz, the delayed phase between $r(t)$ and $r_\infty(t)$ is larger than that between $w(t)$ and $w_\infty(t)$. At the depolarization resonance frequency 342 Hz, the delayed phase between $r(t)$ and $r_\infty(t)$ is much larger than that between $w(t)$ and $w_\infty(t)$, and $r(t)$ becomes small to a larger extent, whereas $w(t)$ to a smaller extent.

3) Especially, $w(t)$ oscillates around $w_\infty(V_{\text{rest}})$, which is consistent with the common view. However, $r(t)$ does not oscillate around $r_\infty(V_{\text{rest}})$ for a relatively high frequency but runs at a level higher than $r_\infty(V_{\text{rest}})$, which is an interesting phenomenon different from the common view, due to $r(t)$ is slow while $w(t)$ is fast.

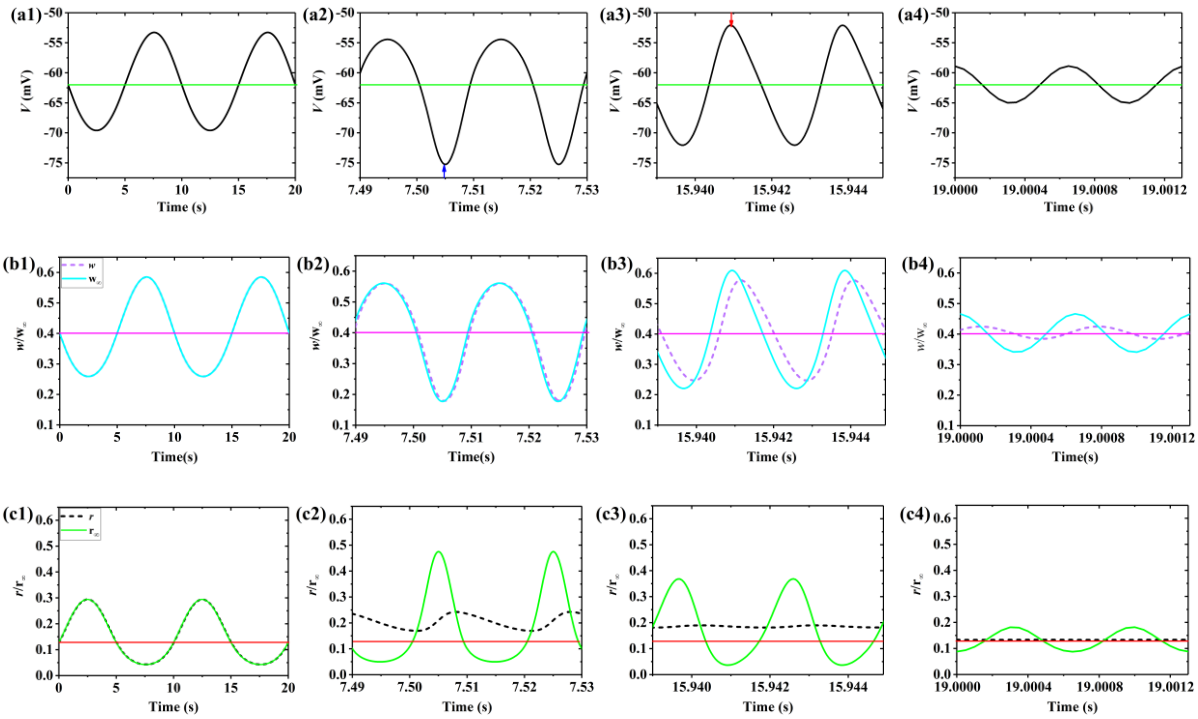

Figure 9. $V(t)$ (top), $w(t)$ and $w_\infty(t)$ (upper), and $r(t)$ and $r_\infty(t)$ (lower) at different frequencies for a strong stimulation $A = 0.7$ nA. (a1), (b1) and (c1): 0.1 Hz; (a2), (b2) and (c2): 50 Hz; (a3), (b3) and (c3): 342 Hz; (a4), (b4) and (c4): 1500 Hz. The solid black curve and green line in the top row represent $V(t)$ and V_{rest}, respectively. The purple dashed and cyan curves represent $w(t)$ and $w_\infty(t)$, respectively. The black dashed and green solid curves represent $r(t)$ and $r_\infty(t)$, respectively. The magenta and red horizontal lines represent $w_\infty(V_{\text{rest}})$ and $r_\infty(V_{\text{rest}})$, respectively. The blue and red arrows indicate hyperpolarization and depolarization resonance, respectively.

3.4. Geometric analysis of symmetrical characteristics of the single and double resonances

The geometrical analysis results at the four different f values are shown in Figure 10. The results in the (w^4, V) plane are shown in the upper panel. In each panel, the three magenta curves from left to right represent V-nullclines ($C_m \dfrac{dV}{dt} = \sum I + A = 0$) or $A = -0.7$ nA, 0 nA, and 0.7 nA, the cyan curve represents the nullcline $w^4 = w_\infty^4(V)$, and the blue curve denotes the phase trajectory of the response behavior. Then, the middle V-nullcline (magenta solid curve) intersects with $w^4 = w_\infty^4(V)$ to form the equilibrium point with $V = V_{\text{rest}}$. And the results in the phase plane (V, r) are shown in the lower row. In each panel, in addition to the three V-nullcline curves depicted by the magenta curves and phase trajectory shown by the blue curve, the green curve denotes the nullcline $r = r_\infty(V)$. Then, the middle V-nullcline (magenta solid) intersects with $r = r_\infty(V)$ to form the equilibrium point with $V = V_{\text{rest}}$.

3.4.1. Single resonance: nearly symmetrical dynamics in a small region around the equilibrium point and with a linear nullcline

Obviously, in each panel, the nullclines are nearly linear within the small range, a V-nullcline exhibits nearly symmetry on the two sides of the w^4–nullcline, and V-nullclines for $A = 0.05$ nA and $A = -0.05$ nA are nearly symmetrical to the equilibrium point and the V-nullcline for $A = 0$ nA. The phase trajectory runs in a small region around the equilibrium point and exhibits symmetry to V_{rest} corresponding to the equilibrium point. The results in the (V, r) plane exhibit behavior similar to those in the (V, w^4) plane.

For the very low frequency such as 0.1 Hz, the phase trajectory in the (V, w^4) plane moves cyclically (anticlockwise) along the w^4–nullcline, around the equilibrium, and within the range between the V-nullclines of $A = 0.05$ nA and $A = -0.05$ nA, due to that w nearly equals w_∞, as depicted in Figure 10(a1). At 50 Hz, the phase trajectory becomes a cycle due to the phase delay between $w(t)$ and $V(t)$ ($w_\infty(t)$), as shown in Figure 10(a2). The phase point runs along the phase trajectory in an anticlockwise. At resonance frequency 243 Hz, the size of the cycle becomes largest due to the optimal phase delay and the largest $V(t)$ values, as shown in Figure 10(a3). At 1500 Hz, the phase trajectory shrinks, as shown in Figure 10(a4), due to the small oscillations of $w(t)$ and $V(t)$. With increasing frequency, the cycle of the phase trajectory rotates in a clockwise direction, from a direction along w^4-nullcline to a direction nearly parallel to the V-axis, due to the enhanced phase delay between $w(t)$ and $V(t)(w_\infty(t))$.

As shown in Figures 10(b2)–(b4), the phase trajectory (V, r) exhibits shrinkage in the r direction, and becomes nearly parallel to the V-axis. At a not low frequency (>50 Hz), the rotation angle of the cycle of the phase trajectory in the V- r plane is larger than that in V- w^4 plane, showing a larger phase delay between $r(t)$ and $r_\infty(t)$, due to the slower frequency response. The direction of the lower row is inverse to the upper row.

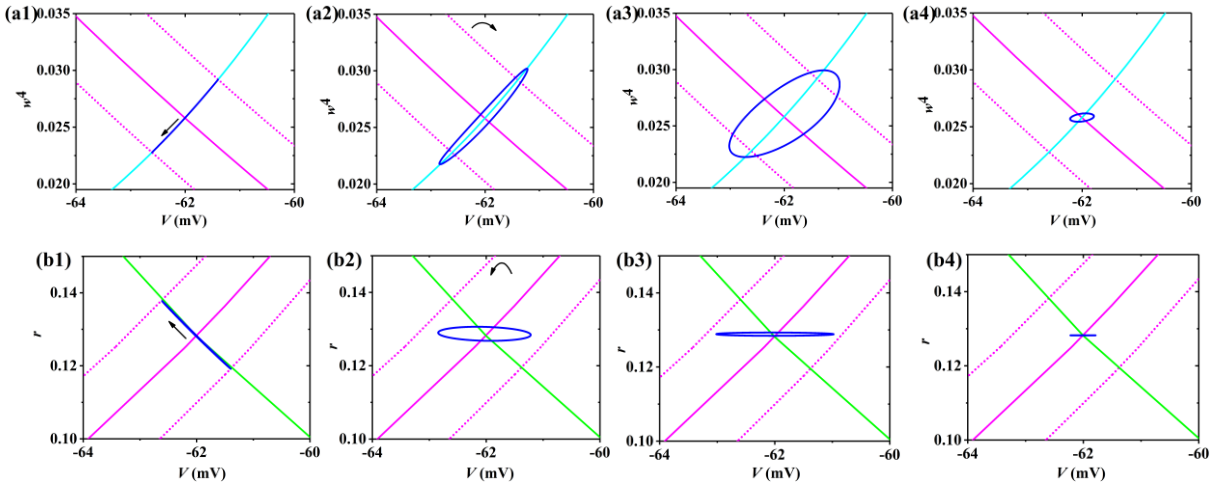

Figure 10. Dynamics in the V-w^4 plane (upper row) and V-r plane (lower row) at the four frequencies for $A = 0.05$ nA. (a1) and (b1): 0.1 Hz; (a2) and (b2): 50 Hz; (a3) and (b3): 243 Hz; (a4) and (b4): 1500 Hz. In each panel, the three magenta solid curves from left to right represent the V-nullcline for $-A$, 0, and A, respectively, the cyan curve denotes the w^4-nullcline, the green curve represents the r-nullcline, blue curve represents the phase trajectory. Upper row: The anti-clockwise arrow represents the phase point running along the phase trajectory, and the arrow with a clockwise direction denotes the rotation of the cycle of the phase trajectory with increasing frequency. Lower row: The direction is inverse to the upper panel.

3.4.2. Double resonances: non-symmetrical dynamics in a large region with nonlinear nullcline

With increasing A to 0.7 nA, the distance between V-nullclines for A and $-A$ becomes larger, the size of the phase trajectory becomes large, V-nullclines, r-nullcline, and w^4-nullcline exhibit strong nonlinearity around the range of the phase trajectory, and V-nullclines for A and $-A$ are asymmetrical to the equilibrium point and V-nullcline for $A = 0$. All these enhance the asymmetrical amplitude on two sides of the equilibrium point (V_{rest}), resulting in enhanced asymmetrical degree with increasing stimulation amplitude. Especially, in the plane V-w^4, the largest size of the phase trajectory appears at the frequency of resonance mediated by the I_{KLT}, as shown by the third column of Figure 11.

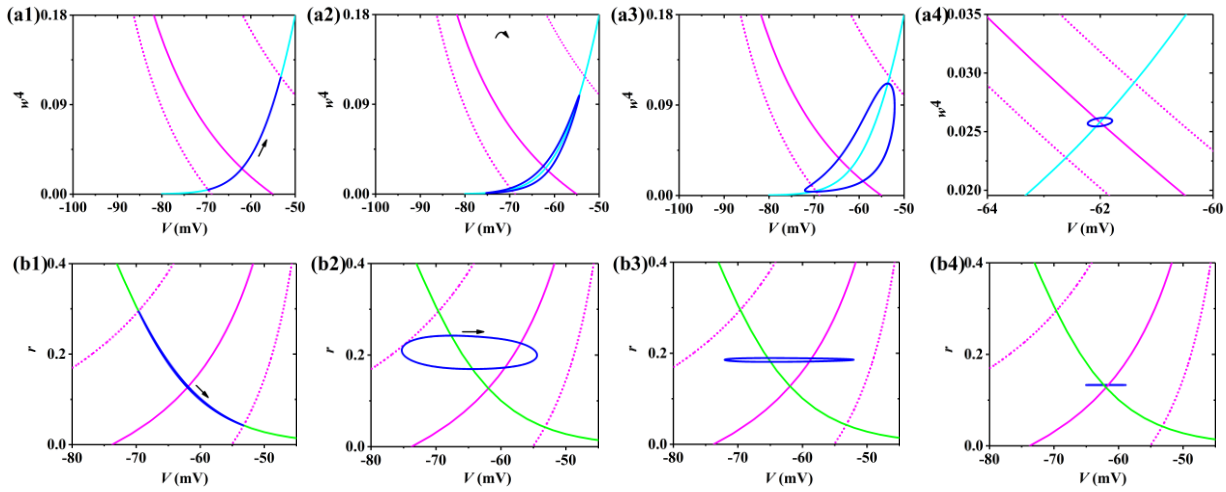

Figure 11. Dynamics in the V-w^4 plane (upper row) and V-r plane (lower row) at the four frequencies for $A = 0.7$ nA. (a1) and (b1): 0.1 Hz; (a2) and (b2): 50 Hz; (a3) and (b3): 342 Hz; (a4) and (b4): 1500 Hz. In each panel, the three magenta solid curves from left to right represent the V-nullcline for $-A$, 0, and A, respectively, the cyan curve denotes the w^4-nullcline, the green curve represents the r-nullcline, blue curve represents the phase trajectory. Upper row: The anti-clockwise arrow represents the phase point running along the phase trajectory, and the arrow with the clockwise direction denotes the rotation of the cycle of the phase trajectory with increasing frequency. Lower row: The direction is inverse to the upper panel.

As shown in Figures 11(b2),(b3), an interesting phenomenon for $r(t)$ (green) for $A_{in} = 0.7$ nA appears. For the fast stimulation with large amplitude, $r(t)$ is higher than r at the equilibrium point, $r_\infty(V_{\text{rest}})$. Such a result is very interesting, since it is not similar to the general view that oscillations should run around the equilibrium point. The phenomenon was reported in the study [27]. In [27], the interesting phenomenon is explained with the narrow region between two nullclines. In the present paper, no small region between nullclines is found in the phase plane. The slow response of $r(t)$ at a high frequency is the cause of the interesting phenomenon, which is addressed in the following subsection.

3.4.3. Oscillations not around equilibrium point: Slow responses of $r(t)$ at high frequency of stimulation

As frequency is changed from 0.1 Hz to 850 Hz, the change of $r(t)$ and $r_\infty(t)$ are shown by the

green and blue curves, respectively, and the red horizontal line represents $r_\infty(V_{\text{rest}})$, as shown in Figure 12. The bottom horizontal axis indicates time, and the top axis shows the exponentially increasing frequency of the I_{ZAP} stimulus over time. Specifically, 0.1 Hz corresponds to the initial time point, 20 s corresponds to 9.2 Hz, and 850 Hz corresponds to 40 s. As shown in Figure 12, $r(t)$ (green curve) oscillates around $r_\infty(V_{\text{rest}})$ (red line) for $t < \sim 24$ s ($f < \sim 22.8$Hz). Within this interval, $r(t)$ keeps up with $r_\infty(t)$ (blue curve) for $t < \sim 13$ s ($f < \sim 2$ Hz), and $r(t)$ cannot keep up with $r_\infty(t)$ for $\sim 13 < t < \sim 24$ s ($\sim 2 < f < \sim 22.8$ Hz).

However, as the stimulus frequency continues to increase, $r(t)$ does not oscillate around $r_\infty(V_{\text{rest}})$ (red line) for $t > \sim 24$ s ($f > \sim 22.8$ Hz), different from the common view that $r(t)$ should oscillate around $r_\infty(V_{\text{rest}})$. Such a phenomenon is observed for the activation variable of the I_M to mediate a resonance in [27]. In the present paper, we extend the phenomenon to the I_H and the activation variable r. In fact, this phenomenon occurs because $r(t)$ is initially too slow to follow $r_\infty(t)$ ($t > 13$ s, $f > 2$ Hz), and then does not oscillate around $r_\infty(t)$ (V_{rest}) at high frequency ($t > 24$ s, $f > 22.8$ Hz). Such a phenomenon does not appear for the variable $w(t)$, due to the fast dynamics of $w(t)$.

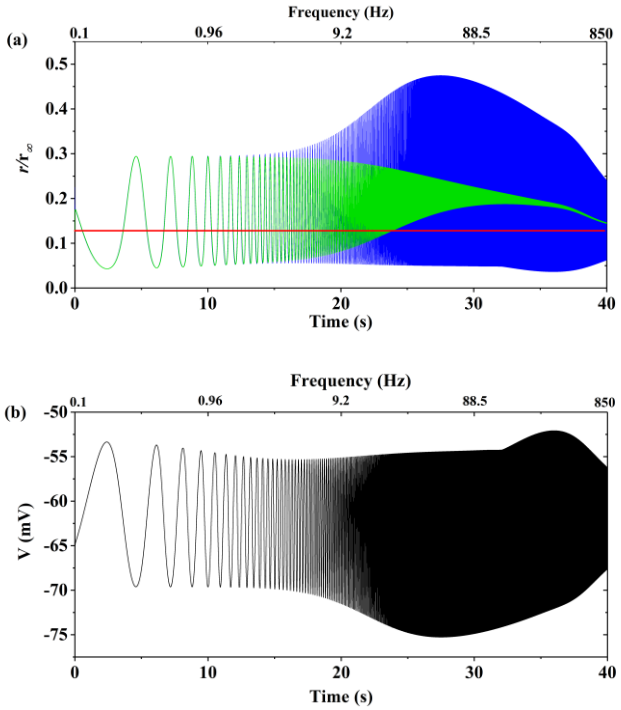

Figure 12. Double resonances with asymmetrical amplitude induced by I_{ZAP} current. As frequency is changed from 0.01 Hz to 850 Hz. (a) The change of $r(t)$ (green) and $r_\infty(t)$ (blue) for A_{in} = 0.7 nA; (b) The voltage. The red horizontal line represents steady state $r_\infty(V_{\text{rest}})$. The frequency is 9.2 Hz at about 20 s.

3.5. Resonance for approximate time scales of I_{KLT} and I_H and strong stimulation

In Subsection 3.2, double resonances with asymmetrical amplitudes for strong stimulation are mediated by a slow current (I_H) and a fast current (I_{KLT}), with $\alpha_H = 0.2$ and $\beta_{KLT} = 0.11$. In Subsection 3.4.3, oscillation not around equilibrium point of slow variable r(t) but around equilibrium point of fast variable w(t) appears at high frequency of stimulation. In the present subsection, I_{KLT} and I_H with approximate time scale, i.e., $\alpha_H = 0.01$ and $\beta_{KLT} = 0.23$, are considered, as shown in Figure 13. The

dashed red and green curves represent τ_r for I_H and τ_w for I_{KLT}, respectively. τ_r approximates τ_w. Then, nearly single resonance with nearly symmetrical amplitude appears, even of the I_{ZAP} stimulation is large (i.e., the paradoxical oscillation shown in Figure 12 disappears). The results are different from those for slow I_H and fast I_{KLT} ($\alpha_H = 0.2$ and $\beta_{KLT} = 0.11$) in subsections 3.2–3.4, showing complex dynamics of resonance related to fast/slow ionic current or time scale.

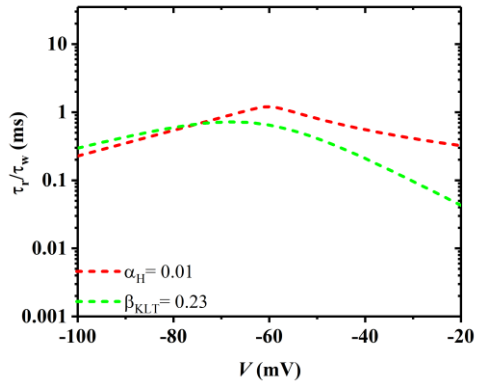

Figure 13. The changes of time constant τ_r for $\alpha_H = 0.01$ (red dashed) of the I_H and τ_w for $\beta_{KLT} = 0.23$ (green dashed) of the I_{KLT} with respect to V.

3.5.1 Nearly symmetrical and single resonance

The voltage response to strong stimulation amplitude $A_{in} = 0.7$ shows single resonance with nearly symmetric amplitude, as depicted in Figure 14(a). The impedance profiles of the upper and lower envelopes of the voltage are shown in Figure 14(b). The peaks of impedance profiles $Z(f)^+$and $Z(f)^-$ appear at nearly the same frequency (i.e., nearly single resonance). The amplitudes $Z(f)^+$and $Z(f)^-$ approximate. $|Z(f)^- - Z(f)^+|$ shown by the magenta curve in Figure 14(b) is very small (< 3), showing nearly symmetrical resonance.

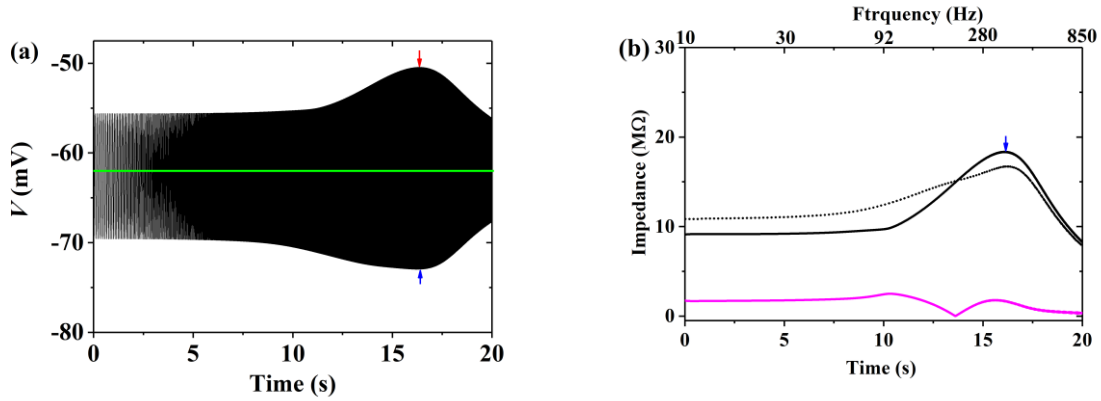

Figure 14. Single resonance with nearly symmetry for $A = 0.7$ nA, $\alpha_H = 0.01$, and $\beta_{KLT} = 0.23$. (a) Voltage response (black curve). The green line represents V_{rest}; (b) Impedance profiles of panel (a). The black solid and dashed curves represent $Z(f)^+$ and $Z(f)^-$, respectively, and the magenta solid curve represents $|Z(f)^- - Z(f)^+|$.

3.5.2 The similar frequency response of $w(t)$ and $r(t)$

At four representative f values of stimulation with A = 0.7 nA, 0.1 Hz, 50 Hz, 368 Hz, and 1500 Hz, the dynamic responses of voltage V, $w(t)$ (purple dashed curve) and $w_\infty(t)$ (cyan solid curve), and $r(t)$ (black dashed curve) and $r_\infty(t)$ (green solid curve) are shown in the top, middle, and bottom rows of Figure 15. Resonance appears at $f \approx$ 368 Hz. Different from Figure 8 to show frequency responses of symmetrical resonance with small amplitude and Figure 9 to show frequency responses of double resonances, wherein $w(t)$ has a faster frequency response than $r(t)$, $w(t)$ exhibits frequency response similar to that of $r(t)$. At $f \approx$ 368Hz, $w(t)$ has a large oscillation amplitude and a middle phase delay to $w_\infty(t)$, and $r(t)$ exhibits similar dynamics. The nearly symmetrical resonance results from the interactions between the I_{KLT} current and the I_H current with nearly the same time constant.

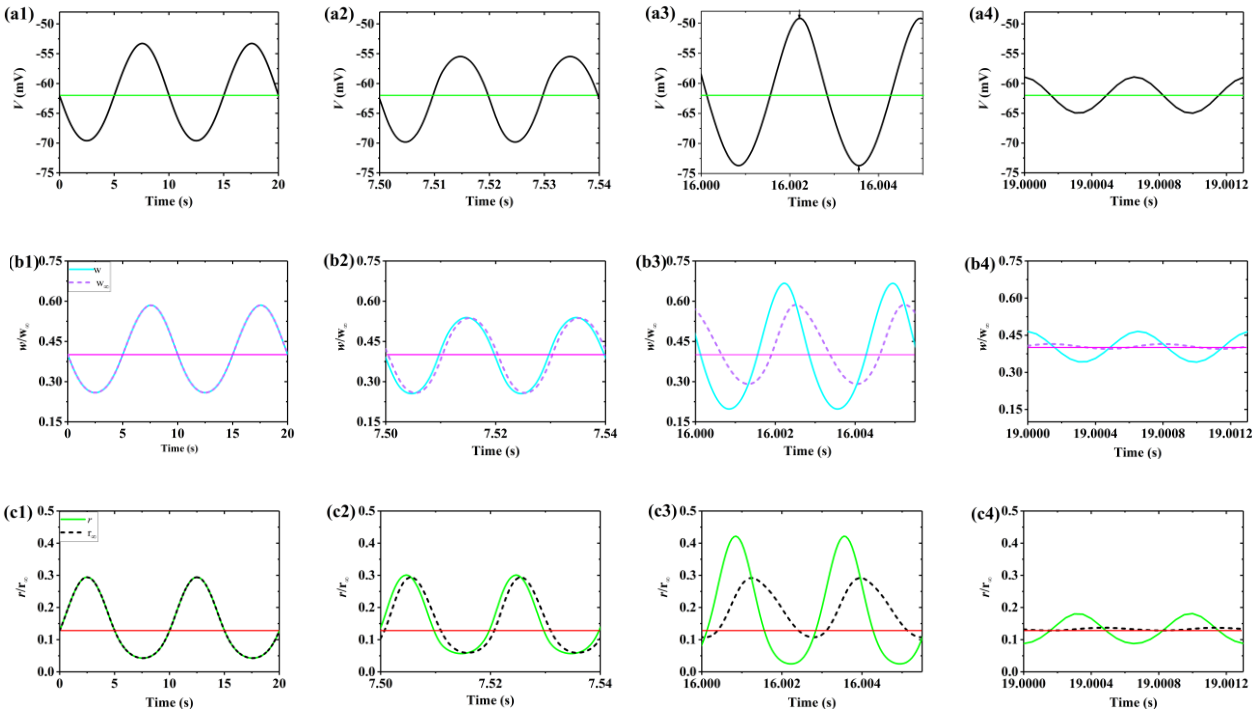

Figure 15. The dynamic processes of voltage $V(t)$ (upper), $w(t)$ (middle), and $r(t)$ (lower) at different frequencies for A = 0.7 nA. (a1), (b1), and (c1): 0.1 Hz; (a2), (b2), and (c2): 50 Hz; (a3), (b3), and (c3): 368 Hz; (a4), (b4), and (c4): 1500 Hz. The black solid represents voltage; The purple dashed and cyan curves represent variable w and steady-state function w_∞, respectively; The black dashed and green curves represent variable r and steady-state function r_∞, respectively.

3.5.3 Dynamics in phase planes: Symmetrical amplitude and oscillations around equilibrium points

Dynamics in the V–w^4 and V–r planes at four representative frequencies are shown in Figure 16. Importantly, it can be found that the largest size of phase trajectory in plane V–w^4 and V–r appears at the same frequency, as shown in the third column, due to that the resonance is single resonance appearing at the frequency. In addition, although the nullclines exhibit nonlinear characteristics

and the phase trajectory runs around the equilibrium point, the ranges of the phase trajectory on two sides of the equilibrium point are nearly equal, showing nearly symmetrical resonance, due to that w and r exhibit nearly the same frequency response. The nearly symmetrical characteristics are different from asymmetrical characteristics in Subsection 3.4, where w and r exhibit different frequency responses.

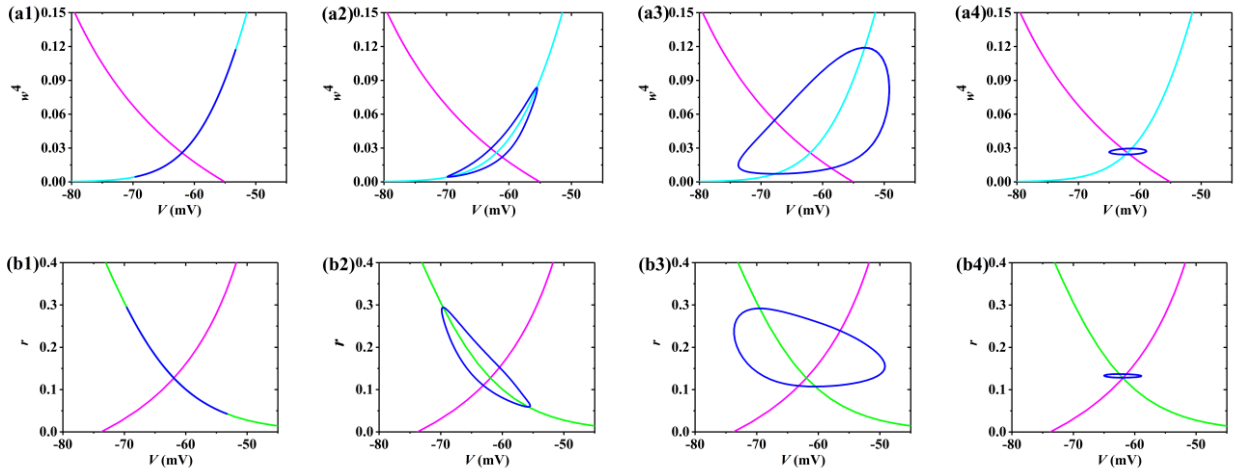

Figure 16. Dynamics in the V– w^4 plane (upper) and V– r plane (lower) at four frequencies for A = 0.7 nA. (a1) and (b1): 0.1 Hz; (a2) and (b2): 50 Hz; (a3) and (b3): 368 Hz; (a4) and (b4): 1500 Hz. In each panel, the three magenta solid curves from left to right represent the V-nullcline for $-A$, 0, and A, respectively, the cyan curve represents the w^4-nullcline, the green curve represents the r-nullcline, and the blue curve represents the phase trajectory.

3.5.4 Oscillations around equilibrium points of $r(t)$ and $w(t)$

As frequency is changed from 0.1 Hz to 850 Hz, the changes in $r(t)$ and $r_\infty(t)$ are shown in Figure 17, where 10 Hz corresponds to approximately 20 s. When $t < 27$ s ($f < 44$ Hz), $r(t)$ (green curve) and $r_\infty(t)$ (blue curve) remain nearly synchronized, as shown in Figure 17(a). Then, $r(t)$ fails to keep up with $r_\infty(t)$ and oscillates around $r_\infty(V_{\text{rest}})$ (red curve) during $27 < t < 36.3$ s ($44 < f < 368$ Hz), with continuously increasing amplitude. Finally, when $t > 36.3$ s ($f > 368$ Hz), $r(t)$ continues to oscillate around $r_\infty(V_{\text{rest}})$ (red curve), but the amplitude gradually decreases. The result differs from Figure 12, due to that the time scale factor α_H of the I_H current reduces from 0.2 to 0.01, resulting in approximate time scale of I_{KLT} and I_H. The changing trends in $w(t)$ and $w_\infty(t)$ are similar to $r(t)$ and $r_\infty(t)$, as shown in Figure 17(b).

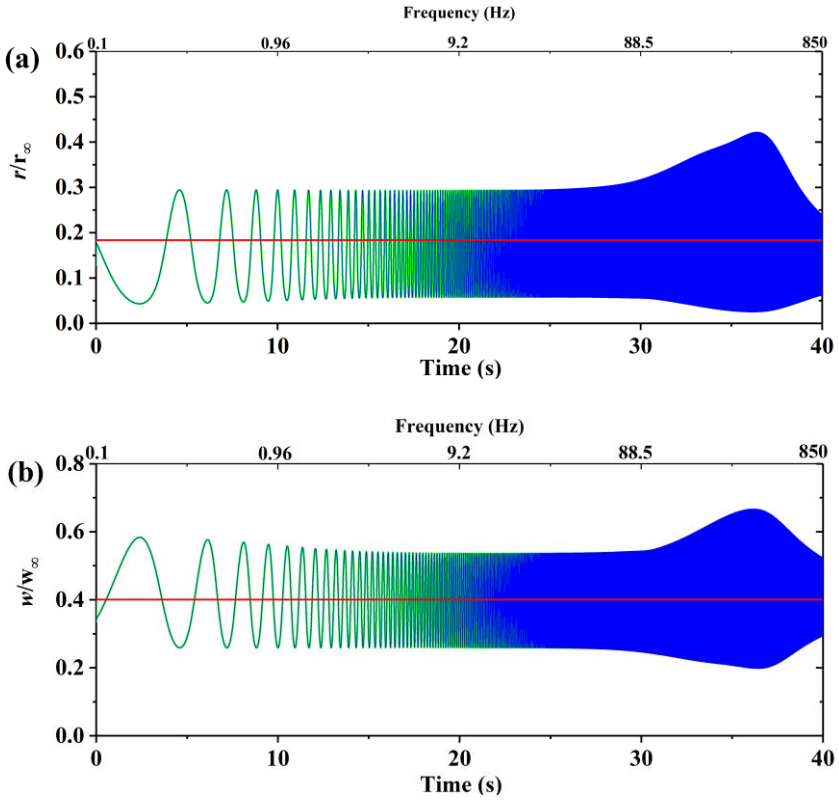

Figure 17. Single resonance with nearly symmetry for $A = 0.7$ nA, $\alpha_H = 0.01$, and $\beta_{KLT} = 0.23$. (a) The change of $r(t)$ (green) and $r_\infty(t)$ (blue); (b) The change of $w(t)$ (green) and $w_\infty(t)$ (blue). The red horizontal line represents steady state $r_\infty(V_{\text{rest}})$.

3.5.5 The dependence of paradoxical oscillation not around steady state on α_H and β_{KLT}

On the parameter plane (α_H, β_{KLT}), $r(t)$ oscillates around the equilibrium point in the yellow region, and $r(t)$ does not oscillate around the equilibrium point in the cyan region. The upper (red) and lower (magenta) stars denote the values of parameters α_H and β_{KLT} corresponding to Figures 12 and 17, respectively. In the range $0.10 < \beta_{KLT} < 0.17$, $r(t)$ oscillates around the equilibrium point for $\alpha_H < 0.01$, and does not oscillate around the equilibrium point for $\alpha_H > 0.01$. In the range $0.17 < \beta_{KLT} < 0.35$, $r(t)$ oscillates around the equilibrium point for $\alpha_H \leq 0.01$, and does not oscillate around the equilibrium point for $\alpha_H > 0.01$. The time scale, phase delay, and ionic dynamics underlying the paradoxical oscillation not around steady state should be studies in future.

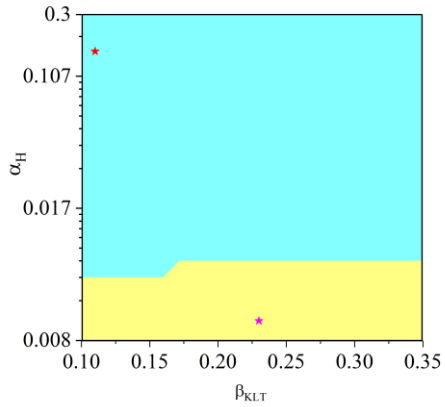

Figure 18. The dependence of oscillations of $r(t)$ around the equilibrium point on α_H and β_{KLT}. The yellow area corresponds to the oscillation of $r(t)$ around the equilibrium point, while the cyan area represents the situation where $r(t)$ does not oscillate around the equilibrium point. The upper (red) and lower (magenta) stars denote the values of parameters α_H and β_{KLT} corresponding to Figures 12 and 17, respectively.

4. Conclusions and discussion

Resonance is an important nonlinear phenomenon in the nervous system, which is involved in information processing through frequency response. Resonance with the high frequency of the MSO neuron contributes to sound localization. Experiments have revealed different resonance patterns in the MSO neuron: single resonance with symmetrical amplitude for a weak stimulation [7], and double resonances with asymmetrical amplitude for a strong stimulation [26]. In the present paper, the nonlinear cooperation mechanisms between ionic currents with different frequency responses for these different resonance patterns are obtained, exhibiting significance in the following aspects.

Firstly, the intrinsic and external conditions for different resonance patterns are obtained. Especially, the level of the V_{rest} is identified, which is a basic factor to recognize the resonance. For the MSO neurons, the activation of I_{KLT} and I_H, the level of resting potential (V_{rest}), and the fast/slow dynamics or high/low frequency response of I_{KLT} and I_H present the intrinsic conditions. The level of V_{rest} presents a key condition for the different resonance patterns, which has not been stated clearly in the previous studies. Based on the simulation result of the resonance closely matching the experimental observation [26,30], V_{rest} is identified to be close to the half-activation voltage of I_{KLT} and far from the half-activation voltage of I_H. If V_{rest} is close to the half-activation potential of I_H, depolarization resonance should appear at first with increasing stimulation amplitude. The timescale of I_{KLT} current activation is significantly faster than that of I_H current. Based on the intrinsic conditions, the weak stimulation induces single resonance, and the strong stimulation evokes double resonances, which present external conditions for the different resonance patterns. Almost all conditions are consistent with experimental conditions [7,26].

Secondly, different resonance patterns are evoked by different stimulation amplitudes, and the stimulation amplitude may be favor of sound localizations. In the previous studies, the single and double resonances were studied independently [7,26]. The strong or weak stimulation to evoke single

or double resonances have not been stated clearly. In the present paper, for weak stimulation, a single resonance with small and symmetrical amplitude is induced, similar to the experiments [7] and the most well-known subthreshold resonance [11]. The resonance exhibits high frequency for sound localization. For strong stimulation, double resonances with large and asymmetrical amplitudes are evoked, similar to the experiment [26]. Furthermore, the high frequency resonance manifests increased frequency with increasing stimulation amplitude, showing precise sound localization. The asymmetrical amplitude of double resonances is a phenomenon that was rarely reported in previous studies [31–33]. Furthermore, the small or large amplitudes of stimulation are obtained, which are dependent of the time scale of ionic current.

Thirdly, different resonance modes are explained with the cooperations of the frequency responses of I_{KLT} and I_H. In the previous studies [7,26,30], the cooperations for the single resonance have not been addressed. In the present paper, at weak stimulation, I_{KLT} is activated whereas I_H current remains in a low activation state, since the level of V_{rest} is close to half-activation of I_{KLT}. Thus, the single resonance is dominated by the rapid frequency response of the I_{KLT} current. However, for strong stimulation, the activation level of the I_H current significantly increases. Then, I_H can mediate a low frequency, and can increase the frequency of resonance mediated by I_{KLT}, forming the double resonances. The cooperation between the slow frequency response of the I_H and the fast response of the I_{KLT} induces the double resonances, which have been partially addressed in a previous study [30].

Fourthly, the geometric method is extended to explain the symmetrical or asymmetrical amplitudes of the different resonance patterns mediated by two ionic currents. In a previous study [27], the asymmetrical amplitude induced by only one ionic current is explained with one nullcline. In the present paper, two nullclines related to I_{KLT} and I_H are considered. For the symmetrical amplitude which is small, the phase trajectory runs in a narrow range around the steady state. The dynamics such as two nullclines exhibit nearly linear and symmetrical characteristics, which are the cause for the symmetrical amplitude. The two nullclines are for w^4 related to I_{KLT} and r associated with I_H, different from only one nullcline in the study [27]. For the asymmetrical amplitude which is large, the phase trajectory runs in a wide range, within which two nullclines manifest asymmetry and strong nonlinearity. Furthermore, the enhanced asymmetrical degree is induced by the increase of the stimulation amplitude, due to the enlarged size of the phase trajectory.

Finally, a paradoxical or interesting phenomenon that the oscillation is not around the steady state is observed, and the fast-slow dynamics underlying the phenomenon is discussed. In a previous study [27], such a paradoxical phenomenon induced by the I_M is reported. However, the mechanism for the phenomenon remains unclear. In the present paper, a slow oscillation that is not around the steady state of the slow variable is induced by stimulation with high frequency, presenting complex nonlinear dynamics underlying the resonances modulated by two ionic currents. At a high frequency stimulation, the oscillation does not run around the steady state of the variable r, which exhibits slow dynamics related to I_H. At the high stimulation frequency, the oscillation amplitude of the slow $r(t)$ cannot keep up with $r_\infty(t)$ within in period. By reducing the time constant of the I_H current, thereby accelerating the I_H current, resulting in approximate time scale of I_{KLT} and I_H. Then, the paradoxical oscillation disappears, and recovers to revolve around the steady state, which presents fast-slow or time scale dynamics of the paradoxical or interesting phenomenon.

In summary, the results present the dynamics of the different resonance patterns caused by different stimulus amplitudes in the MSO neuron, which is not only helpful to understand frequency responses for sound localization, but also to understand the nonlinear phenomena across in engineering

and natural sciences [34,35]. In future, more dynamic behaviors associated with sound localization should be investigated, particularly the post-inhibition facilitation (PIF) in the MSO neurons related to the fast dynamics of I_{KLT} current [14,36], as well as the post-inhibitory rebound (PIR) phenomenon in the superior paraolivary nucleus (SPN) neurons modulated by the I_H current [37]. In addition, the geometric analysis method combined with frequency response may be used to explain subthreshold resonance in other neuronal types, such as the inferior olive [21]. However, resonance in inferior olive neurons is largely governed by T-type calcium current, differing markedly from the I_{KLT}. The difference should be considered when geometric analysis method is used to analyze the resonance induced by T-type calcium current. Furthermore, a mathematical model from the perspective of phase delay and current feedback should be proposed to fully explain the essence of the paradoxical phenomenon that $r(t)$ does not oscillate around the steady-state value.

Use of AI tools declaration

The authors declare they have not used Artificial Intelligence (AI) tools in the creation of this article.

Acknowledgments

This work was sponsored by the National Natural Science Foundation of China (Grant No. 11802086), the Wuxi University Research Start-up Fund for High-level Talents (Grant No. 550225093), and the Natural Science Foundation of Inner Mongolia Autonomous Region of China (Grant No. 2021MS01016).

Conflict of interest

The authors declare there are no conflicts of interest.

References

1. H. Zhou, X. Wang, H. Gu, Y. Jia, Deep brain stimulation-induced two manners to eliminate bursting for Parkinson's diseases: synaptic current and bifurcation mechanisms, *Cognit. Neurodyn.*, **19** (2025), 78. https://doi.org/10.1007/s11571-025-10267-5
2. K. Ma, H. Gu, Y. Jia, The neuronal and synaptic dynamics underlying post-inhibitory rebound burst related to major depressive disorder in the lateral habenula neuron model, *Cognit. Neurodyn.*, **18** (2024), 1397–1416. https://doi.org/10.1007/s11571-023-09960-0
3. B. Cao, H. Gu, K. Ma, Complex dynamics of hair bundle of auditory nervous system (I): spontaneous oscillations and two cases of steady states, *Cognit. Neurodyn.*, **16** (2022), 917–940. https://doi.org/10.1007/s11571-021-09744-4
4. S. C. Song, J. A. Beatty, C. J. Wilson, The ionic mechanism of membrane potential oscillations and membrane resonance in striatal LTS interneurons, *J. Neurophysiol.*, **116** (2016), 1752–1764. https://doi.org/10.1152/jn.00511.2016
5. L. Guan, H. Gu, Z. Zhao, Dynamics of subthreshold and suprathreshold resonance modulated by hyperpolarization-activated cation current in a bursting neuron, *Nonlinear Dyn.*, **104** (2021), 577–601. https://doi.org/10.1007/s11071-021-06230-8

6. J. Vera, U. Pereira, B. Reynaert, J. Bacigalupo, M. Sanhueza, Modulation of frequency preference in heterogeneous populations of theta-resonant neurons, *Neuroscience*, **426** (2020), 13–32. https://doi.org/10.1016/j.neuroscience.2019.10.054
7. M. W. H. Remme, R. Donato, J. Mikiel-Hunter, J. A. Ballestero, S. Foster, J. Rinzel, et al., Subthreshold resonance properties contribute to the efficient coding of auditory spatial cues, *Proc. Natl. Acad. Sci. U.S.A.*, **111** (2014), E2339–E2348. https://doi.org/10.1073/pnas.1316216111
8. Y. Wu, Z. Sun, N. Zhao, Resonance dynamics in multilayer neural networks subjected to electromagnetic induction, *Commun. Nonlinear Sci. Numer. Simul.*, **143** (2025), 108575. https://doi.org/10.1016/j.cnsns.2024.108575
9. P. Gastrein, E. Campanac, C. Gasselin, R. H. Cudmore, A. Bialowas, E. Carlier, et al., The role of hyperpolarization-activated cationic current in spike-time precision and intrinsic resonance in cortical neurons in vitro, *J. Physiol.*, **589** (2011), 3753–3773. https://doi.org/10.1113/jphysiol.2011.209148
10. R. Narayanan, D. Johnston, Long-term potentiation in rat hippocampal neurons is accompanied by spatially widespread changes in intrinsic oscillatory dynamics and excitability, *Neuron*, **56** (2007), 1061–1075. https://doi.org/10.1016/j.neuron.2007.10.033
11. B. Hutcheon, Y. Yarom, Resonance, oscillation and the intrinsic frequency preferences of neurons, *Trends Neurosci.*, **23** (2000), 216–222. https://doi.org/10.1016/S0166-2236(00)01547-2
12. E. Stark, A. Levi, H. G. Rotstein, Network resonance can be generated independently at distinct levels of neuronal organization, *PLoS Comput. Biol.*, **18** (2022), e1010364. https://doi.org/10.1371/journal.pcbi.1010364
13. J. Mikiel-Hunter, V. Kotak, J. Rinzel, High-frequency resonance in the gerbil medial superior olive, *PLoS Comput. Biol.*, **12** (2016), e1005166. https://doi.org/10.1371/journal.pcbi.1005166
14. B. Beiderbeck, M. H. Myoga, N. I. C. Müller, A. R. Callan, E. Friauf, B. Grothe, et al., Precisely timed inhibition facilitates action potential firing for spatial coding in the auditory brainstem, *Nat. Commun.*, **9** (2018), 1771. https://doi.org/10.1038/s41467-018-04210-y
15. R. Dodla, G. Svirskis, J. Rinzel, Well-timed, brief inhibition can promote spiking: Postinhibitory facilitation, *J. Neurophysiol.*, **95** (2006), 2664–2677. https://doi.org/10.1152/jn.00752.2005
16. P. J. Mathews, P. E. Jercog, J. Rinzel, L. L. Scott, N. L. Golding, Control of submillisecond synaptic timing in binaural coincidence detectors by K_v1 channels, *Nat. Neurosci.*, **13** (2010), 601–609. https://doi.org/10.1038/nn.2530
17. C. E. Carr, K. M. Macleod, Microseconds matter, *PLoS Biol.*, **8** (2010), e1000405. https://doi.org/10.1371/journal.pbio.1000405
18. B. Grothe, M. Pecka, D. McAlpine, Mechanisms of sound localization in mammals, *Physiol. Rev.*, **90** (2010), 983–1012. https://doi.org/10.1152/physrev.00026.2009
19. S. Khurana, M. W. H. Remme, J. Rinzel, N. L. Golding, Dynamic interaction of Ih and IK-LVA during trains of synaptic potentials in principal neurons of the medial superior olive, *J Neurosci.*, **31** (2011), 8936–8947. https://doi.org/10.1523/JNEUROSCI.1079-11.2011
20. P. Joris, T. C. T. Yin, A matter of time: internal delays in binaural processing, *Trends Neurosci.*, **30** (2007), 70–78. https://doi.org/10.1016/j.tins.2006.12.004
21. Y. Matsumoto-Makidono, H. Nakayama, M. Yamasaki, T. Miyazaki, K. Kobayashi, M. Watanabe, et al., Ionic basis for membrane potential resonance in neurons of the inferior olive, *Cell Rep.*, **16** (2016), 994–1004. https://doi.org/10.1016/j.celrep.2016.06.053

22. D. Ulrich, Subthreshold delta-frequency resonance in thalamic reticular neurons, *Eur. J. Neurosci.*, **40** (2014), 2600–2607. https://doi.org/10.1111/ejn.12630
23. H. Hu, K. Vervaeke, J. F. Storm, Two forms of electrical resonance at theta frequencies, generated by M-current, h-current and persistent Na^+ current in rat hippocampal pyramidal cells, *J. Physiol.*, **545** (2002), 783–805. https://doi.org/10.1113/jphysiol.2002.029249
24. P. Mishra, R. Narayanan, Ion-channel degeneracy: Multiple ion channels heterogeneously regulate intrinsic physiology of rat hippocampal granule cells, *Physiol. Rep.*, **9** (2021), e14963. https://doi.org/10.14814/phy2.14963
25. S. Schreiber, I. Erchova, U. Heinemann, A. V. M. Herz, Subthreshold resonance explains the frequency-dependent integration of periodic as well as random stimuli in the entorhinal cortex, *J. Neurophysiol.*, **92** (2004), 408–415. https://doi.org/10.1152/jn.01116.2003
26. L. Fischer, C. Leibold, F. Felmy, Resonance properties in auditory brainstem neurons, *Front. Cell. Neurosci.*, **12** (2018), 8. https://doi.org/10.3389/fncel.2018.00008
27. R. F. O. Pena, V. Lima, R. O. Shimoura, C. C. Ceballos, H. G. Rotstein, A. C. Roque, Asymmetrical voltage response in resonant neurons shaped by nonlinearities, *Chaos*, **29** (2019), 103135. https://doi.org/10.1063/1.5110033
28. C. F. Shay, I. S. Boardman, N. M. James, M. E. Hasselmo, Voltage dependence of subthreshold resonance frequency in layer II of medial entorhinal cortex, *Hippocampus*, **22** (2012), 1733–1749. https://doi.org/10.1002/hipo.22008
29. Z. Zhao, L. Li, H. Gu, Dynamical mechanism of hyperpolarization-activated non-specific cation current induced resonance and spike-timing precision in a neuronal model, *Front. Cell. Neurosci.*, **12** (2018), 62. https://doi.org/10.3389/fncel.2018.00062
30. R. Wang, H. Gu, X. Zhang, Dynamics of interaction between IH and IKLT currents to mediate double resonances of medial superior olive neurons related to sound localization, *Cognit. Neurodyn.*, **18** (2024), 715–740. https://doi.org/10.1007/s11571-023-10024-6
31. D. M. Fox, H. A. Tseng, T. G. Smolinski, H. G. Rotstein, F. Nadim, Mechanisms of generation of membrane potential resonance in a neuron with multiple resonant ionic currents, *PLoS Comput. Biol.*, **13** (2017), e1005565. https://doi.org/10.1371/journal.pcbi.1005565
32. K. Hashimoto, Mechanisms for the resonant property in rodent neurons, *Neurosci. Res.*, **156** (2020), 5–13. https://doi.org/10.1016/j.neures.2019.12.013
33. J. Vera, M. Pezzoli, U. Pereira, J. Bacigalupo, M. Sanhueza, Electrical resonance in the θ frequency range in olfactory amygdala neurons, *PLoS One*, **9** (2014), e85826. https://doi.org/10.1371/journal.pone.0085826
34. T. Li, Y. V. Rogovchenko, Oscillation criteria for second-order superlinear Emden–Fowler neutral differential equations, *Monatsh. Math.*, **184** (2017), 489–500. https://doi.org/10.1007/s00605-017-1039-9
35. T. Li, D. Acosta-Soba, A. Columbu, G. Viglialoro, Dissipative gradient nonlinearities prevent δ-formations in local and nonlocal attraction–repulsion chemotaxis models, *Stud. Appl. Math.*, **154** (2025), e70018. https://doi.org/10.1111/sapm.70018
36. R. Wang, H. Gu, Y. Li, Nonlinear mechanism for paradoxical facilitation of spike induced by inhibitory synapse in auditory nervous system for sound localization, *Nonlinear Dyn.*, **112** (2024), 19393–19419. https://doi.org/10.1007/s11071-024-10008-z

37. E. Rajaram, C. Kaltenbach, M. J. Fischl, L. Mrowka, O. Alexandrova, B. Grothe, et al., Slow NMDA-mediated excitation accelerates offset-response latencies generated via a post-inhibitory rebound mechanism, *eNeuro*, **6** (2019), e0106-19. https://doi.org/10.1523/ENEURO.0106-19.2019